


## Article

# Variability in Mechanical Properties and Cracking Behavior of Frozen Sandstone Containing En Echelon Flaws under Compression

Weimin Liu <sup>1</sup>, Li Han <sup>2,\*</sup>, Di Wu <sup>2</sup>, Hailiang Jia <sup>2</sup>  and Liyun Tang <sup>2</sup><sup>1</sup> CCCC First Highway Consultants Co., Ltd., Xi'an 710075, China; liuweimin1@ccccltd.cn<sup>2</sup> College of Architecture and Civil Engineering, Xi'an University of Science and Technology, Xi'an 710054, China; wdjg@xust.edu.cn (D.W.); hailiang.jia@xust.edu.cn (H.J.); tangly@xust.edu.cn (L.T.)

\* Correspondence: hanli@stu.xust.edu.cn

**Abstract:** The mechanical properties of frozen fissured rock masses are crucial considerations for engineering in frozen earth. However, there has been little research on the mechanical properties of frozen fissured sandstone, including its strength, deformation, and geometric parameters. In this study, sandstone samples with three open en echelon fissures were observed using high-speed photography and acoustic emissions during uniaxial compression tests. The aim was to investigate sandstone's strength, deformability, and failure process in order to elucidate the effects of freezing on its mechanical properties. In the frozen-saturated and dried states, the uniaxial compression strength (UCS) initially decreases and then increases with an increase in fissure inclination angle. Conversely, the UCS of samples in the saturated state continuously increases. The UCS follows a decreasing trend, as follows: frozen-saturated state > dried state > saturated state. The initial crack angle decreases as the fissure inclination increases in all states, irrespective of temperature and moisture conditions. However, the initial crack stress and time show an increasing trend. The uniaxial compression strength (UCS) of frozen fissured sandstone is influenced by four mechanisms: (1) ice provides support to the rock under compression, (2) ice fills microcracks, (3) unfrozen water films act as a cementing agent under tension or shearing loads, and (4) frost damage leads to softening of the rock.



**Citation:** Liu, W.; Han, L.; Wu, D.; Jia, H.; Tang, L. Variability in Mechanical Properties and Cracking Behavior of Frozen Sandstone Containing En Echelon Flaws under Compression. *Appl. Sci.* **2024**, *14*, 3427. <https://doi.org/10.3390/app14083427>

Academic Editor: Dibyendu Sarkar

Received: 4 February 2024

Revised: 1 March 2024

Accepted: 16 April 2024

Published: 18 April 2024



**Copyright:** © 2024 by the authors. Licensee MDPI, Basel, Switzerland. This article is an open access article distributed under the terms and conditions of the Creative Commons Attribution (CC BY) license (<https://creativecommons.org/licenses/by/4.0/>).

**Keywords:** uniaxial compression; frozen fissured sandstone; crack coalescence; crack initiation

## 1. Introduction

In high-altitude and high-latitude regions, the underground rock can be frozen to depths of several hundred meters [1]. The stability of frozen rock masses during excavation and mining poses challenges for engineering in such areas [2–4]. The natural rock mass contains numerous joints and fissures of various types, which directly influence its strength, deformability, and geometric parameters. Therefore, studying the mechanical properties of frozen fissure sandstone holds significant engineering value.

Most research on fissured rock masses has been conducted at room temperature. The characteristics of the rock and the geometric parameters of its fissures have a coupled effect on the strength of a fissured rock mass [5–10], which tends to decrease with increases in both fissure length and width [11]. Additionally, the number of fissures also influences the strength of the rock mass; a higher number of fissures leads to lower initial crack stress and failure strength compared to rocks with fewer fissures [12,13]. Moreover, as the inclination increases, the uniaxial compression strength (UCS) curve exhibits a decreasing trend followed by an increasing trend, reaching its minimum value at an inclination angle of 30° [14,15]. Furthermore, the fissure type also has an important influence on strength. The strength of a rock mass containing parallel fissures is influenced by the inclination and distribution of the fissures, as well as the length and angle of the rock bridge, which

can lead to various modes of crack coalescence [16–19]. In fact, seven types of cracks have been defined for single-fissure-containing rock masses, while the types of crack coalescence are recognized to be combinations of these seven basic crack types [20–24]. Lastly, it is worth noting that experimental results may be influenced by factors such as filler type and volume within rock fissures; however, overall similarities exist between crack coalescence patterns observed in filled versus unfilled-rock-mass-containing fissures [25,26].

There has been extensive research conducted on rock mechanical properties at freezing temperature; however, limited studies have been carried out specifically on fissured rock masses. The mechanical properties of frozen rock are significantly influenced by factors such as freezing temperature, moisture content, and pore structure. The strength of frozen porous rock increases as the freezing temperature decreases [27]. The strength of frozen porous rock decreases initially with increasing moisture content, then increases, and finally decreases again [28]. Additionally, freeze–thaw cycling also impacts the mechanical properties of rock masses, with the strength decreasing as the number of cycles increases [29–33]. Research on frozen fissured rock masses has recently emerged as a focal point of investigation. The ultrasonic acoustic characteristics, local damage, and tip fractures in fissured rock masses during freeze–thaw cycling have been extensively studied [34,35]. However, there is still a need to investigate the mechanical properties of fissured rock masses at freezing temperatures. Furthermore, it is imperative to explore the mechanism behind the enhancement of freezing in frozen fissure rock mass.

The present research conducted experiments to investigate the mechanical properties of fissured rock masses at freezing temperature, specifically focusing on uniaxial compressive strength, strain, and elastic modulus. The failure process was observed using a high-speed camera and acoustic emissions in samples with fissures inclined at five different angles. The mechanism behind the enhancement of strength due to freezing is thoroughly explained. The objective of this research was to examine the mechanical properties and cracking behavior of frozen fissured sandstone, providing valuable insights for safe rock engineering in frozen underground environments. Section 2 will provide an overview of the basic physical characteristics of specimens and details regarding the experimental procedure; Section 3 will focus on presenting the uniaxial compression strength characteristics of fissured sandstone; Section 4 will showcase the acoustic emissions during the compression process; and Section 5 will illustrate the failure process of fissured sandstone under uniaxial compression.

## 2. Methodology

### 2.1. Specimens and Equipment

The experimental specimen was course-grained quartz sandstone with a porosity of 19.58%, a natural water content of 0.24%, a bulk density of 1.57 g/cm<sup>3</sup>, and a P-wave velocity of 2.67 km/s. The specimen was Cretaceous sandstone and classified as Lacustrine sediments. Its main mineral components were quartz (53.8%), feldspar (27.4%), calcite (11.2%), and dolomite (7.6%). The sandstone plates were precisely cut to dimensions of 160 mm × 120 mm × 20 mm with an accuracy of ±1 mm. They contained three open en echelon fissures with five different inclination angles (15°, 30°, 45°, 60°, and 75°). The length of the fissure, *L*, was measured at 22 mm, the width, *W*, was 1.30 mm, and the rock bridge length, *H*, was 20 mm with a stationary angle of 90°. The three parallel fissures were designated as Nos. 1, 2, and 3. The inclination was defined as the angle between the fissure and the horizontal direction (Figure 1).

A uniaxial compression experiment was conducted using an electro-hydraulic servo-system with a constant-temperature environmental chamber. The press ram employed in the electro-hydraulic servo-system was constructed using fiberglass, thereby exhibiting inadequate thermal conductivity. It was placed across the top of the chamber and made contact with the specimen installation equipment (Figure 2). Throughout the experiment, the chamber door remained closed, while the compression process was observed through

a window in it. The specimen installation equipment was independently designed and consisted of three components: an upper plate, a bottom plate, and four guide columns.

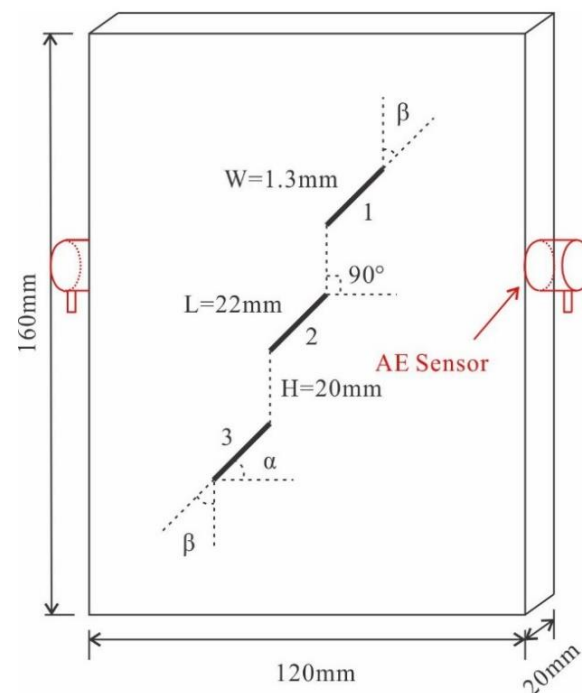


**Figure 1.** Schematic of a fissured sandstone specimen.

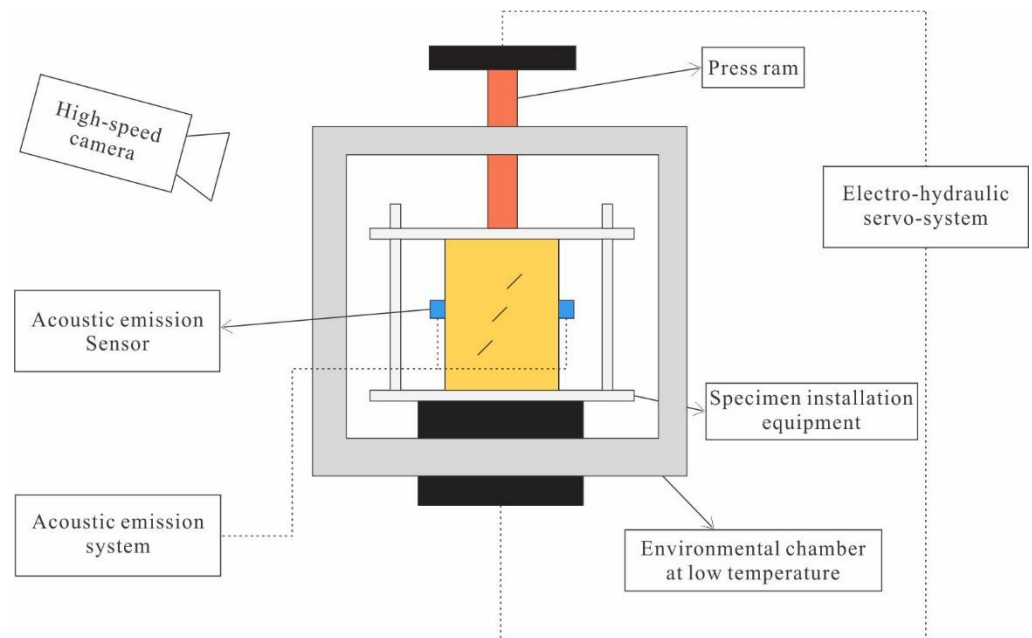


**Figure 2.** Schematic of the experimental apparatus.

## 2.2. Experimental Design

Specimens with fissure inclinations of  $15^\circ$ ,  $30^\circ$ ,  $45^\circ$ ,  $60^\circ$ , or  $75^\circ$  were subjected to uniaxial compression tests under three different conditions: dried ( $25^\circ\text{C}$ ), saturated ( $25^\circ\text{C}$ ), and frozen-saturated ( $-20^\circ\text{C}$ ). The objective was to gain insights into the failure characteristics of frozen fissure sandstone in relation to the inclination angle of the fissure and frost. The process was as follows:

1. Place the specimens in a drying oven set at  $105^\circ\text{C}$  for a duration of 24 h.

2. Subject the specimens to a vacuum chamber with a negative pressure of  $-1$  atmosphere for a period of 2 h, followed by immersion in water until their mass stabilizes.
3. Transfer the specimens to a cryogenic freezing box maintained at  $-20$  °C for 6 h.
4. Introduce the specimens into an environmental chamber and maintain them at  $-20$  °C for 2 h.
5. Begin the uniaxial compression experiment and observe the process using high-speed photography and acoustic emission monitoring. During this process, record the load and deformation using an electro-hydraulic servo-system, and then calculate the data for each specimen, presented as a stress–strain curve in Figure 3. The peak strength and strain values from Figure 3 are collected and displayed in Figure 4, along with the calculation of elastic modulus. The acoustic characteristics of specimens during the failure process are recorded using an acoustic emission device, with both acoustic emission events and axial strain exhibited in Figure 7. The cracking process of each specimen is captured by a high-speed camera, with initial cracks shown in Figure 10, while the failure process of three states is illustrated in Figures 11–13. The entire experiment is divided into two parts: pre-pressure (1 kN) stage and formal experiment (loading rate = 30 kN/min) stage; an environmental chamber is utilized to maintain a constant temperature for the specimens.

### 3. Uniaxial Compression Strength Characteristics of Fissured Sandstone

#### 3.1. Stress–Strain Curves

The stress–strain curves of fissured sandstone are influenced by factors such as fissure inclination, temperature, and saturation. Figure 3 illustrates the stress–strain curves for the five samples in different states: dried (Figure 3a), saturated (Figure 3b), and frozen-saturated (Figure 3c). It is evident that the stress–strain curves exhibit three distinct stages: pore closure (A), elastic deformation (B), and crack propagation (C). Fissure inclination plays a critical role in determining both the UCS and failure strain of fissured sandstone.

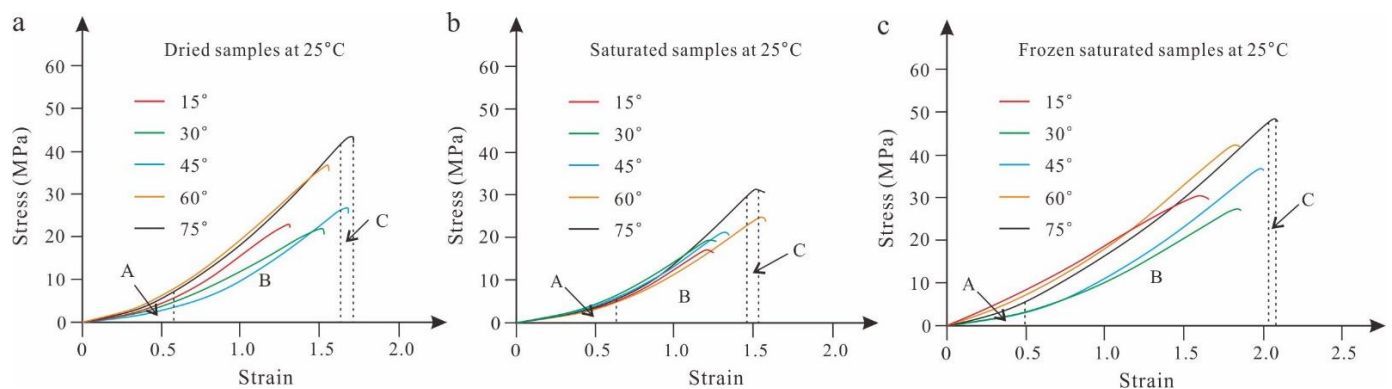


**Figure 3.** Stress–strain curves under (a) dried, (b) saturated, and (c) frozen-saturated conditions.

#### 3.2. Strength Characteristics with Fissures of Five Different Inclinations

The strength, failure strain, and elastic modulus of rock are influenced by the inclination of fissures. In the frozen-saturated and dried states, the UCS curve exhibits a decreasing trend followed by an increasing trend with increasing inclination; its minimum value is observed at an inclination of  $30^\circ$ . However, in the saturated state, the curve shows continuous growth (Figure 4a). The UCS values decrease in the following order: frozen saturated state > dried state > saturated state. The failure strain initially increases, then decreases, and finally increases again in both the dried and frozen-saturated states. However, in the saturated state, it first increases and then decreases (Figure 4b). Similar to the UCS values, the failure strains also follow a decreasing trend in the order of frozen-saturated state > dried state > saturated state. The elastic modulus experiences an initial drop followed by a

rise in both the dried and frozen-saturated states, but demonstrates continuous growth in the saturated state.

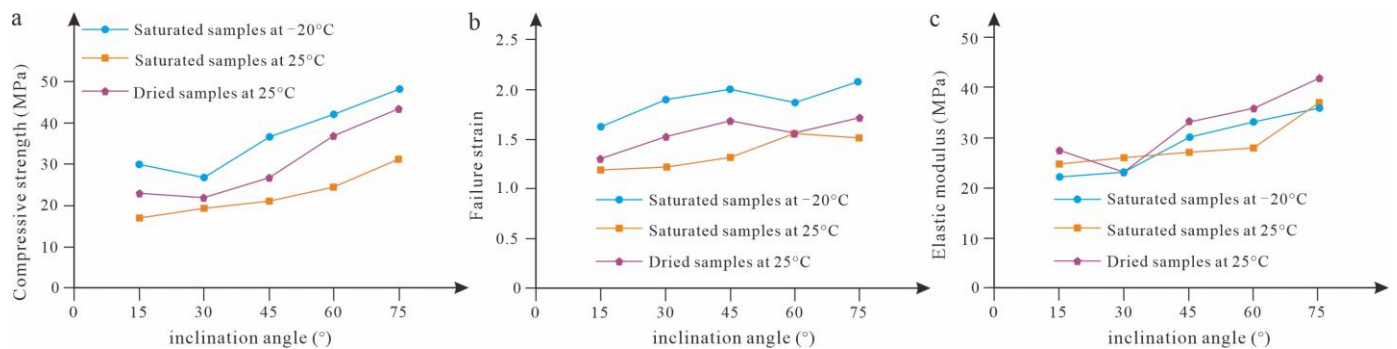


**Figure 4.** Compressive strength (a), failure strain (b), and elastic modulus (c) vs. inclination.

Liu and Li reported a strong correlation between the initial crack stress and strength with the full-field strain evolution as inclination changed [6]. Figure 5 illustrates the strain localization area and its corresponding stress variation with changes in inclination, using digital image correlation (DIC). It can be observed that as inclination increases, the strain localization gradually shifts from the middle to the tip of the fissure. The stress  $\sigma$  at which strain localization occurs also increases with inclination and approaches the specimen's strength  $\sigma_p$ , but only reaches 39.6% of  $\sigma_p$  at an inclination of 30°. This indicates that an inclination of 30° is most conducive to generating strain localization. As the inclination angle becomes higher, it becomes more challenging for strain localization to occur near the fissure, implying greater difficulty in deformation. Consequently, in both frozen-saturated and dried states, there is a downward-upward trend in UCS curve with increasing inclination, reaching its minimum value at an inclination angle of 30°.

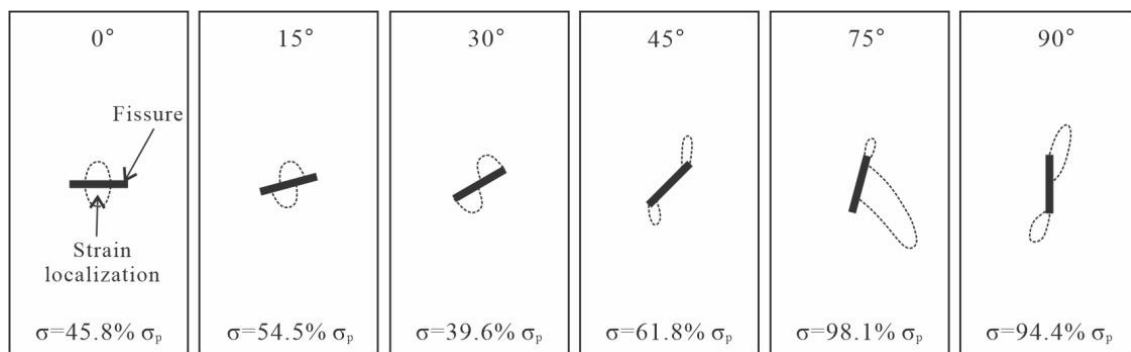


**Figure 5.** Strain localization areas at different fissure inclination angles in the rock materials.

The strength, failure strain, and elastic modulus are also influenced by temperature and saturation state. In the dried state, the UCS of fissured sandstone is higher than that in the saturated state at the same inclination angle, indicating a softening effect caused by water. However, in the frozen-saturated state, the UCS of fissured sandstone is stronger than that in the saturated state, suggesting an increase in UCS due to freezing (Figure 6a). The ranking of UCS can be described as follows: frozen-saturated state > dried state > saturated state. Similarly, the failure strain follows a similar trend: frozen-saturated state > dried state > saturated state (Figure 6b). On the other hand, for inclinations of 45° and 60°, there is a similarity between elastic modulus trends and UCS variations (Figure 6c).

Pore water has a softening effect on sandstone after it is saturated at room temperature. It not only dissolves soluble cementation among mineral grains, but also acts as a lubricant on the rock matrix. These two effects decrease the bonding strength and friction among sandstone mineral grains, leading to a lower UCS in saturated specimens compared to



dried ones. Saturated sandstone exhibits increased UCS after freezing due to the changes in the phase composition of pore water, which reflects the relative amounts of unfrozen water and pore ice. Mechanical interactions among the water, ice, and rock matrix also occur. When subjected to a load, the mechanical properties of frozen rock are influenced by the composition of the pore water phase, as explained by Wang and Sun [36], which is demonstrated as follows:

1. Enhanced support from ice under compression: the sandstone pores tend to close when subjected to uniaxial compression, and the presence of pore ice imparts a supporting force that elevates the strength and modulus of the frozen sandstone.
2. Microcrack-filling effect of ice: the microcracks induced by uniaxial compression are filled with the ice, thereby reducing stress concentrations at the crack tips and enhancing the strength of the rock.
3. Cementing effect of unfrozen water film under tension or under shearing load: the unfrozen water film adheres to the pores, thereby enhancing their resistance against tensile and shear forces.
4. Frost damage effect: the freezing process leads to an expansion in the volume of pore water, which is attributed to the frost heave force exerted on the pores, resulting in the formation of new microcracks among the grains. In other words, the rock matrix undergoes damage due to the frost heave force, leading to a reduction in the strength of the frozen sandstone.

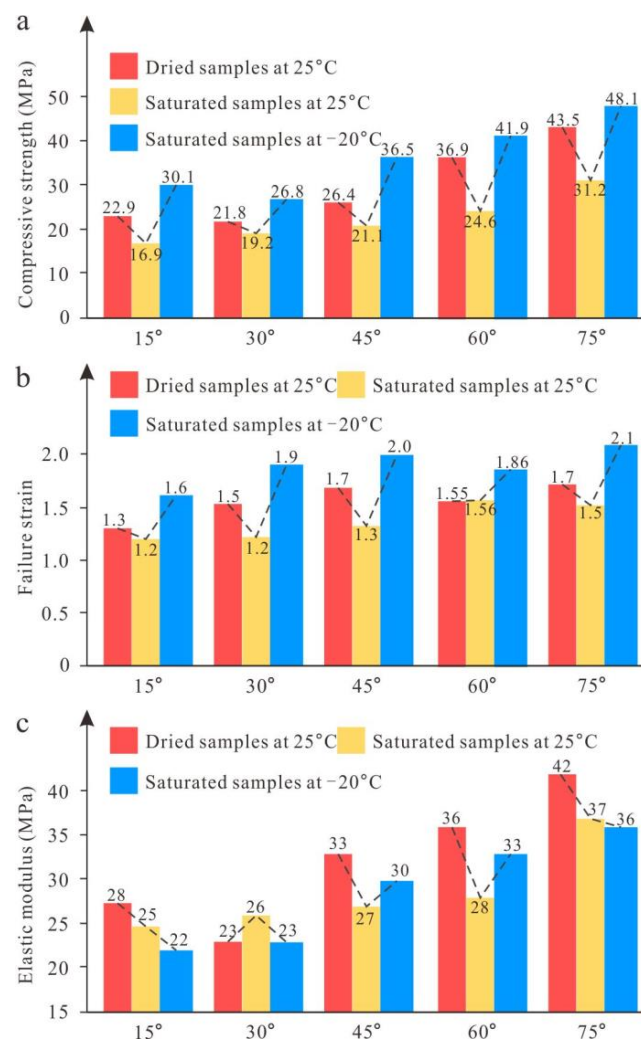


**Figure 6.** Strength ((a) compressive strength; (b) failure strain; (c) elastic modulus) enhancement and softening effects on sandstone with fissures of different inclinations.

The UCS of frozen fissure sandstone is controlled by four distinct effects. Three enhancement effects counteract the softening effect, resulting in an increase in the UCS of fissure sandstone between the saturated and frozen-saturated states.

#### 4. Acoustic Emissions (AEs) of Fissured Sandstone during the Compression Process

##### 4.1. AE Events

Acoustic emissions (AEs) are utilized for the observation of the acoustic characteristics exhibited by fissured sandstone during the process of failure under uniaxial compression. These acoustic signals effectively capture both micro and macro cracking behavior, which correspond to the deformation experienced by the specimens during uniaxial compression. The analysis focuses on studying the failure process of fissured sandstone through the examination of acoustic emission events in conjunction with axial strain measurements. Figure 7 illustrates the acoustic emission (AE) events during the failure process under conditions of saturated, dried, and frozen-saturated states. The AE event data were pre-processed because of the non-uniform faces of the specimens and adjustments were made to the experimental equipment utilized for generating the AE signal. The figure clearly illustrates that the AE event corresponds to axial strain during the compression process of fissured sandstone, indicating that the peak value of the AE event reflects sudden changes in axial strain. This effectively captures information regarding the initial crack tip, crack propagation, and failure process during the compression process. All of the time–strain curves exhibit similar trends: (1) strain increases over time but at a gradually decreasing rate, and (2) even when reaching the final peak of AE event, some residual strain remains until brittle fracture of the specimen occurs.

Under preliminary compression, the absence of an AE event count indicates the non-propagation of microcracks at this stage. The time of an AE event occurrence increases with the inclination angle in all three states, implying that higher inclination angles result in delayed microcrack appearance. In the dried and frozen-saturated states, there are three peaks of AE events during the compression process: The first peak corresponds to the initial crack formation and propagation between the three fissures near the inner tip; the second peak corresponds to the initial crack formation and propagation in fissures No. 1 and 3 near the outer tip; and the third peak represents specimen failure. However, in the saturated state, there are only two peaks of AE events during the compression process: one corresponding to initial crack formation and propagation between the three fissures near the inner tip, and another corresponding to specimen failure. The magnitude of the AE event peak is lower in the saturated state compared to in dried and frozen-saturated states due to deformation occurring during the compression process; pore water dissolves some mineral constituents, leading to the debonding of mineral grains, resulting in increased porosity. Consequently, continuous energy release occurs as a consequence of rock deformation throughout this process, causing a less significant increase in accumulated energy generating AE events.

The data presented in Figure 7 also demonstrate a clear trend wherein the occurrence time of AE events increases with the inclination angles across all three states. However, it is observed that the appearance time of AE events follows an increasing order for the saturated state, dry state, and freezing-saturated state, corresponding to the initial crack time, which will be further discussed in Section 4.2.

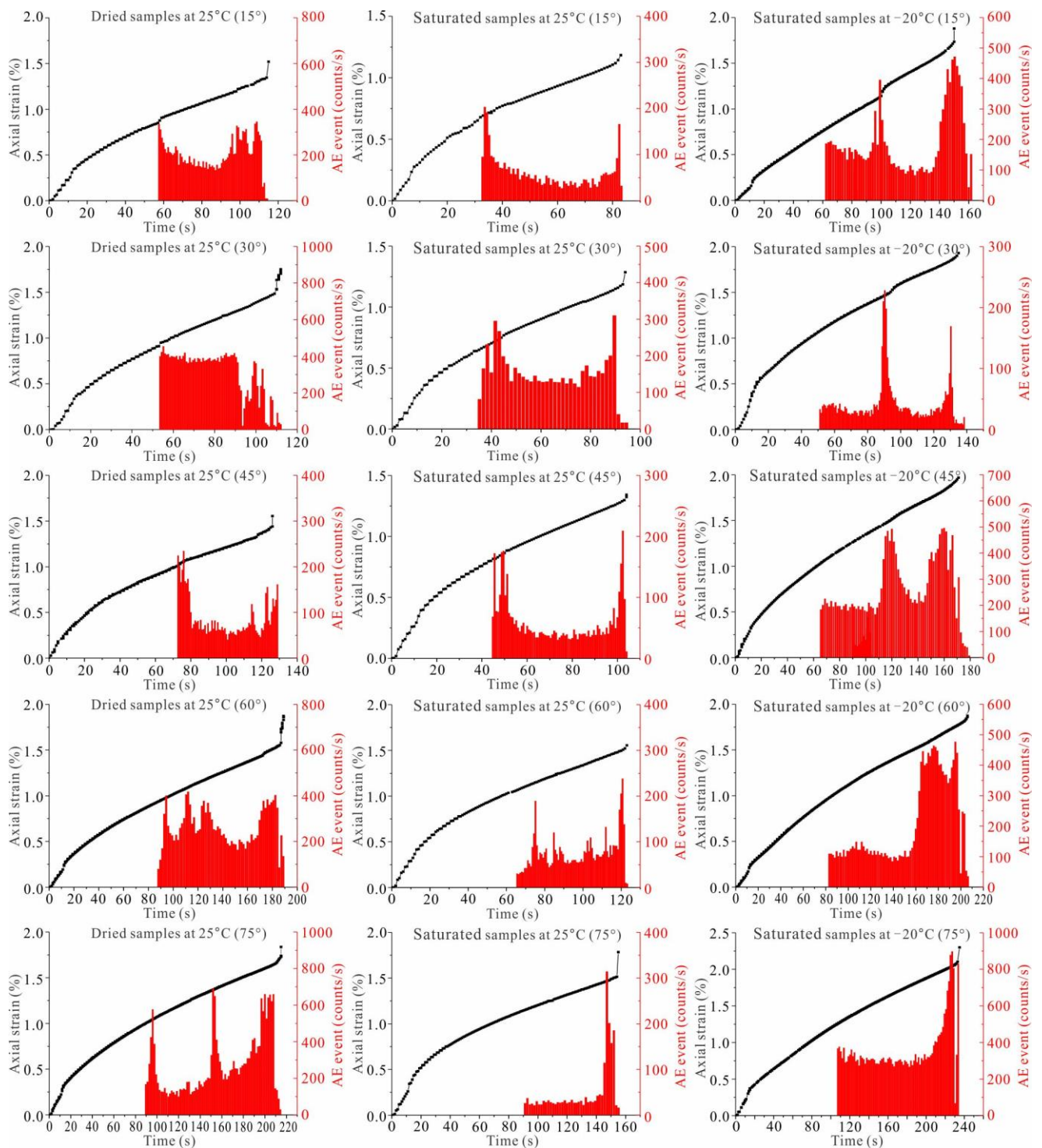


**Figure 7.** AE events and axial strain in dried, saturated, and frozen-saturated states.

#### 4.2. Initial Cracking during the Compression Process

The consideration of the initial crack stress and time is crucial for comprehending the phenomenon of initial cracking during the compression of fissured sandstone. When subjected to axial compression, the tip of the fissure fractures, giving rise to an initial crack. The stress sustained by the sandstone at this moment is defined as the initial crack stress, while the corresponding time is referred to as the initial crack time. The first peak in the AE event corresponds to both the initial crack stress and time during the compression process. Figure 8 illustrates that there is an increase in both initial crack stress and time



with increasing inclination angle in all three states. In a dried state, there is a slight decrease followed by a gradual increase in initial crack stress as inclination angle rises; similarly, the curve for initial crack time exhibits a similar trend to that of initial crack stress. For both saturated and frozen-saturated states, there is a proportional increase in both initial crack stress and time with inclination angle. The ranking order for these parameters at a specific inclination angle can be stated as follows: frozen-saturated state > dried state > saturated state. This implies that the softening effect of pore water and the enhancement due to freezing temperature also influence the initiation of cracks in fissured sandstone.

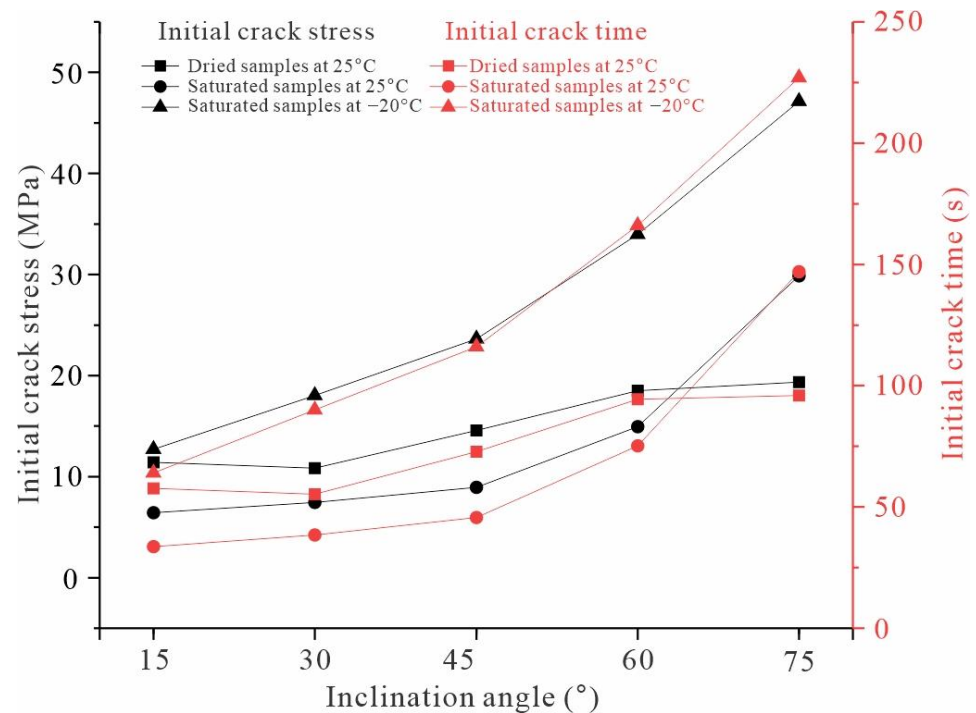


**Figure 8.** Initial crack stress and time at different inclination angles.

The enhancement rate  $F$  is defined as the ratio of the initial crack stress to UCS. This parameter can aid in understanding the relationship between initial crack stress and inclination, and its equation is as follows:

$$F = \frac{R_i}{R_p} \times 100\% \quad (1)$$

where  $R_i$  is the initial crack stress of the fissured sandstone and  $R_p$  is the UCS of fissured sandstone. The data presented in Figure 9 illustrate the relationship between  $F$  and inclination angle across three states. It is evident that  $F$  increases with rising inclination angle in both the saturated and frozen-saturated states, indicating a gradual approach between the initial crack stress and the UCS, and an increased difficulty in initial cracking as inclination rises. This can be attributed to the fact that higher inclination angles impede strain localization near fissures, resulting in a reduced deformation likelihood. Conversely, the enhancement rate  $F$  remains constant at 20% for the dried state regardless of changes in inclination angle. Furthermore, it should be noted that the pore water (ice) enhances the ductility of fissured sandstone while also improving its resistance against fractures.

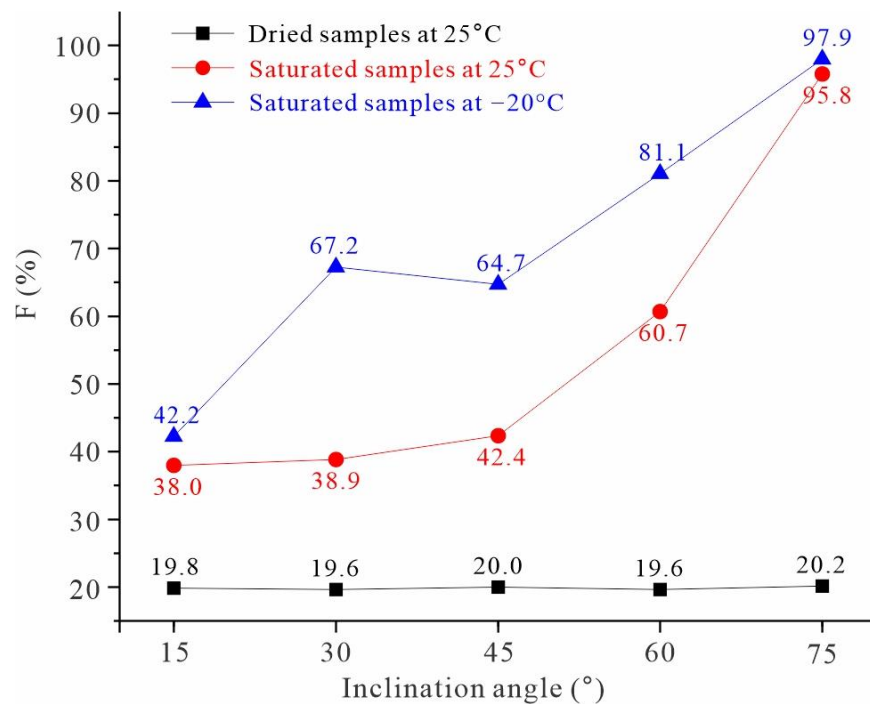


**Figure 9.** Enhancement rate  $F$  vs. inclination angle in the three states.

## 5. Failure Process of Fissured Sandstone under Uniaxial Compression

### 5.1. Initial Crack Angle

The *initial crack angle* is defined as the angle between the fissure and the initial crack. Figure 10 illustrates the characteristics of the initial crack in the three states based on high-speed imagery. To facilitate convenient measurement, black lines were used to highlight the initial cracks in each specimen, and these data are presented in Figure 11. In most specimens, the initial crack exhibited a wing-crack pattern, except for the dried state sample with an inclination of 75°, which displayed an anti-wing-crack pattern. Figure 11 demonstrates how the initial crack angle varies with inclination. It can be observed that as inclination increases, there is a decrease in the angles of these cracks; however, neither temperature nor saturation has any influence on these angles. The reason behind this phenomenon lies in the generation of stress concentration at the tip of the fissure during the compression process. Once this stress concentration reaches an equilibrium with the tensile stress between the sandstone mineral grains, an initial crack emerges at the fissure tip and subsequently generates a wing crack. The direction of crack propagation is determined by the orientation of the major principal stress, which aligns itself with this orientation post-cracking and consequently leads to a reduction in initial crack angles with increasing inclination.

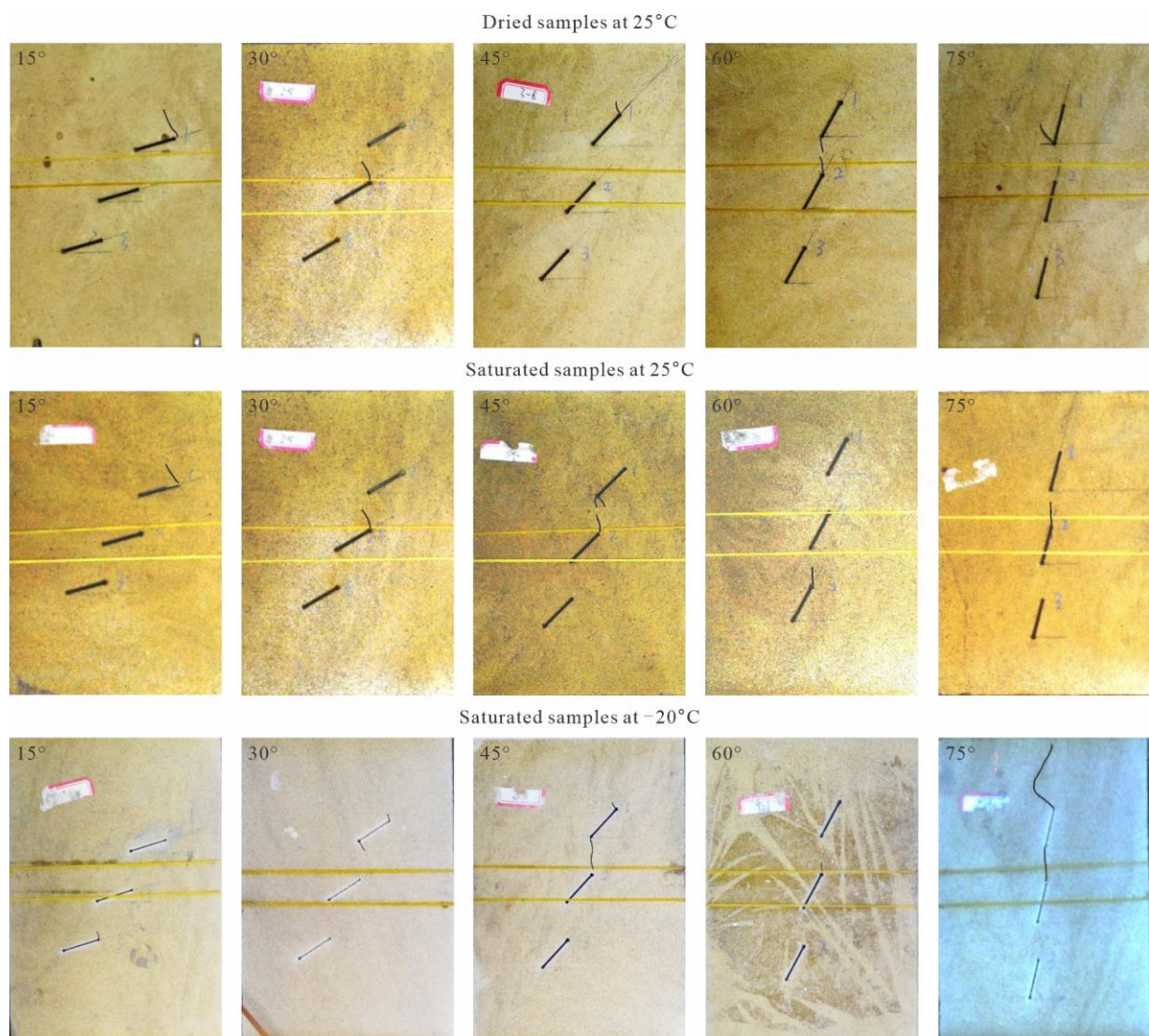


**Figure 10.** High-speed images of initial cracks at various inclination angles under the three states. The numbers (1–3) represent fissure numbers, as illustrated in Figure 1.

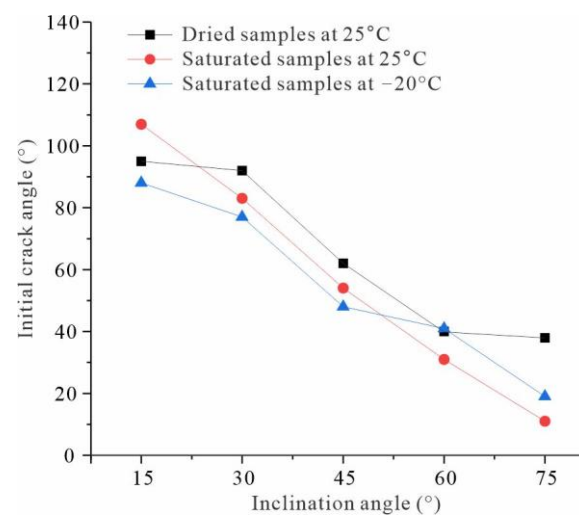


**Figure 11.** Variation in initial crack angle with fissure inclination angle.

## 5.2. Failure Process

The failure process can be categorized into three stages: crack coalescence, initial cracking at the outer fissure tip, and final failure. High-speed photography is employed to observe the failure process in three states using a 45° inclined sample as an example, aiming to comprehend the compression failure process of fissured sandstone. Due to the time span between crack initiation and final failure exceeding the recording capacity of the high-speed camera, the analysis of the failure process is conducted after some time following crack coalescence.

### (1) Dried state

Figure 12 illustrates the process of compression failure in dried fissured sandstone. Stage I: a rock bridge between fissures cracks and coalesces. Stage II: (i) the outer tips of fissures 1 and 3 crack, resulting in a wing crack (first crack); (ii) with an increase in axial load, a shear crack (second crack) and anti-wing crack appear in the outer tip of fissure 1. Stage III: The shear crack in the outer tip of fissure 1 propagates to the top-right direction of the specimen, causing exfoliation damage along with an anti-wing crack. The wing crack in the outer tip of fissure 3 propagates to the bottom of the specimen, causing a complete separation into two parts along the penetrating crack. Subsequently, fissure 1 undergoes nearly complete closure.

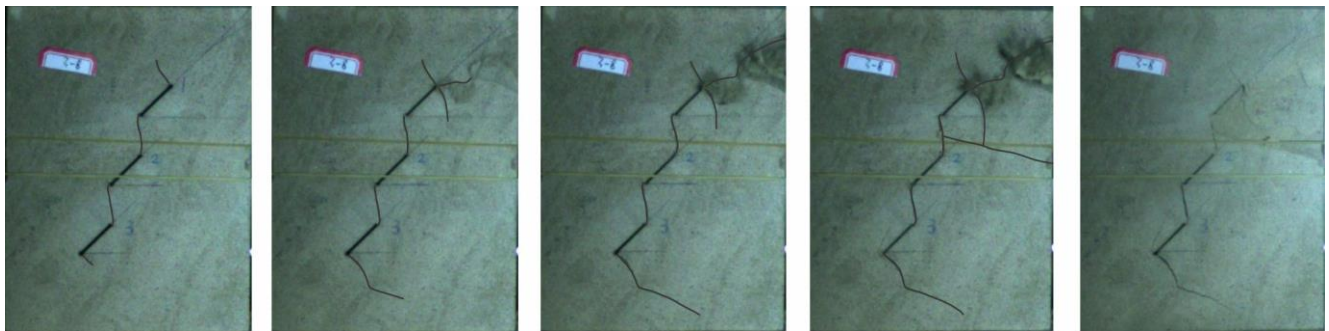


**Figure 12.** Failure process in the dried state. The numbers (1–3) represent fissure numbers, as illustrated in Figure 1.

### (2) Saturated state

Figure 13 illustrates the compression failure process of fissured sandstone in the saturated state. Stage I: a wing crack appears at the inner tip of fissure 1 and propagates towards the upper tip of fissure 2; simultaneously, a wing crack initiates at the bottom tip of fissure 2 and propagates to the upper tip of fissure 3; additionally, a wing crack appears at the inner tip of fissure 3 and propagates in the direction of fissure 2. Stage II: (i) Exfoliation damage occurs as cracks initiate at the outer tips of both fissures 1 and 3, and a tensile crack propagates in the direction of fissure 2; the rock bridge between fissures 2 and 3 is fractured. (ii) With an increase in axial load, a shear crack (second crack) appears at the outer tip of fissure 3, resulting in fracture within the rock bridge connecting fissures 1 and 2. Stage III: the exfoliated damage from fissure 1 extends towards the top-right direction on specimen; meanwhile the shear crack in the outer tip of fissure 3 propagates to the bottom of the specimen, ultimately causing a division into two parts with slip occurring along the penetrating cracks. As a result, almost complete closure is observed for both fissure 1 and fissure 3.

### (3) Frozen-saturated state

Figure 14 illustrates the compression failure process of fissured sandstone in the frozen-saturated state. Stage I: the rock bridge between fissures undergoes cracking and coalescence. Stage II: (i) the outer tip of fissure 1 cracks and a shear crack appears; (ii) with an increase in axial load, the shear crack in the outer tip of fissure 1 propagates upward



and a wing crack appears in the outer tip of Fissure 3 and propagates to the bottom of the specimen; (iii) a wing crack appears in the outer tip of fissure 3 and propagates in the direction of fissure 2. Stage III: the widths of the shear crack in the outer tip of fissure 1 and the tensile crack in the outer tip of fissure 3 increase; consequently, the entire specimen is divided into two parts that slip along a penetrating crack; fissures 1, 2, and 3 almost close.

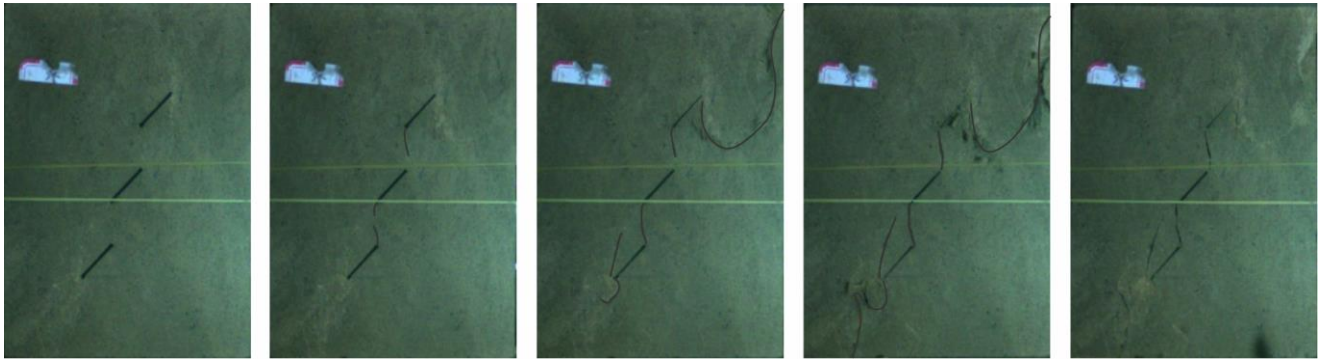


**Figure 13.** Failure process in the saturated state.

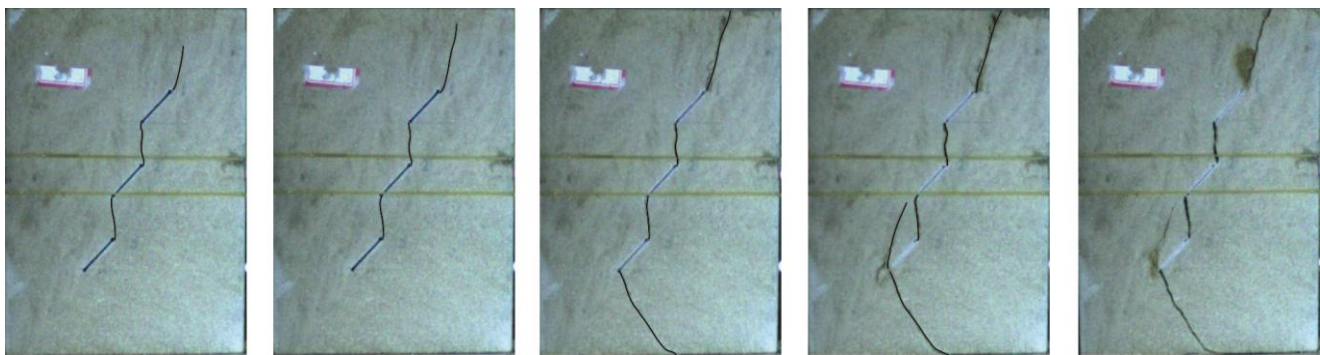


**Figure 14.** Failure process in the frozen saturated state.

## 6. Conclusions

The objective of this research is to investigate the mechanical properties and cracking behavior of frozen fissured sandstone, aiming to provide valuable insights for conducting safe rock engineering in frozen underground rock. High-speed photography and acoustic emissions are employed to observe frozen fissured sandstone with three open en echelon fissures under uniaxial compression. The strength, deformability, and failure processes are thoroughly examined, revealing the influence of freezing on the mechanical properties. The main conclusions are as follows:

1. The mechanical properties are influenced by the inclination angle of fissures, saturation, and temperature. In the frozen-saturated and dried states, the UCS curve decreases first and then increases with an increase in inclination angle, reaching its minimum value at  $30^\circ$ . However, in the saturated state, the UCS shows a continuous increase. The ranking of UCS can be stated as follows: frozen-saturated state > dried state > saturated state.
2. The AE events in the dried and frozen-saturated states exhibit three peaks during the compression process. The first peak corresponds to the initiation of cracking and propagation between the three fissures, while the second peak corresponds to initial cracking and propagation at the outer tip within fissures 1 and 3; the third corresponds to specimen failure. However, in the saturated state, there are only two peaks observed during the compression process. The first peak represents initial cracking and propagation between all three fissures, whereas the second peak indicates specimen failure.



3. The initial crack angles decrease with a rise in fissure inclination, while temperature and saturation have no influence on the initial crack angle. However, the initial crack stress and time increase with fissure inclination in all three states. Furthermore, the ranking of the initial crack stress and time at a given inclination is as follows: frozen-saturated state > dried state > saturated state.
4. The strength of saturated sandstone increases when subjected to freezing, and this phenomenon can be attributed to four underlying mechanisms: (1) ice provides braced force under compression, (2) ice fills microcracks, and (3) an unfrozen water film provides a cementing effect under tension or shearing load, while (4) the frost damage effect causes softening. The first three mechanisms counteract the softening effect, resulting in an increase in the UCS of saturated fissured sandstone during freezing.
5. The mechanical properties and crack behavior of frozen fissured rock containing a single pre-existing flaw, as well as the influence of ice within the flaw on stress distributions at the fissure tip, remain unclear. These aspects require further investigation in future studies.

**Author Contributions:** Conceptualization, W.L. and L.H.; methodology, W.L.; validation, L.T. and D.W.; formal analysis, L.H.; investigation, D.W.; resources, H.J.; data curation, L.H.; writing—original draft preparation, W.L.; writing—review and editing, L.H.; supervision, L.T.; project administration, H.J.; funding acquisition, H.J. All authors have read and agreed to the published version of the manuscript.

**Funding:** This study was funded by the National Natural Science Foundation of China (grant No. 41702334).

**Institutional Review Board Statement:** Not applicable.

**Informed Consent Statement:** Not applicable.

**Data Availability Statement:** The data presented in this study are available on request from the corresponding author. The data are not publicly available due to privacy.

**Conflicts of Interest:** Author Weimin Liu was employed by the company CCCC First Highway Consultants Co., Ltd. The remaining authors declare that the research was conducted in the absence of any commercial or financial relationships that could be construed as a potential conflict of interest.

## References

1. Sammis, C.; Biegel, R. Mechanics of strengthening in crystalline rock at low temperatures: A preliminary assessment. In Proceedings of the 26th Seismic Research Review: Trends in Nuclear Explosion Monitoring, Orlando, FL, USA, 21–23 September 2004; pp. 475–484.
2. Jia, H.; Ding, S.; Zi, F.; Dong, Y.; Shen, Y. Evolution in sandstone pore structures with freeze-thaw cycling and interpretation of damage mechanisms in saturated porous rocks. *CATENA* **2020**, *195*, 104915. [\[CrossRef\]](#)
3. Ma, L.; Qi, J.; Yu, F.; Yao, X. Experimental study on variability in mechanical properties of a frozen sand as determined in triaxial compression tests. *Acta Geotech.* **2016**, *11*, 61–70. [\[CrossRef\]](#)
4. Xu, X.; Li, Q.; Xu, G. Investigation on the behavior of frozen silty clay subjected to monotonic and cyclic triaxial loading. *Acta Geotech.* **2019**, *15*, 1289–1302. [\[CrossRef\]](#)
5. Liu, L.; Li, H.; Li, X.; Wu, D.; Zhang, G. Underlying mechanisms of crack initiation for granitic rocks containing a single pre-existing flaw: Insights from digital image correlation (Dic) analysis. *Rock Mech. Rock Eng.* **2020**, *54*, 857–873. [\[CrossRef\]](#)
6. Liu, L.; Li, H.; Li, X.; Wu, R. Full-field strain evolution and characteristic stress levels of rocks containing a single pre-existing flaw under uniaxial compression. *Bull. Eng. Geol. Environ.* **2020**, *79*, 3145–3161. [\[CrossRef\]](#)
7. Park, C.; Bobet, A. Crack initiation, propagation and coalescence from frictional flaws in uniaxial compression. *Eng. Fract. Mech.* **2010**, *77*, 2727–2748. [\[CrossRef\]](#)
8. Wong, L.N.Y.; Xiong, Q. A method for multiscale interpretation of fracture processes in carrara marble specimen containing a single flaw under uniaxial compression. *J. Geophys. Res. Solid Earth* **2018**, *123*, 6459–6490. [\[CrossRef\]](#)
9. Morgan, S.P.; Johnson, C.A.; Einstein, H.H. Cracking processes in Barre granite: Fracture process zones and crack coalescence. *Int. J. Fract.* **2013**, *180*, 177–204. [\[CrossRef\]](#)
10. Vásárhelyi, B.; Bobet, A. Modeling of crack initiation, propagation and coalescence in uniaxial compression. *Rock Mech. Rock Eng.* **2000**, *33*, 119–139. [\[CrossRef\]](#)

11. Liu, T.; Lin, B.; Zheng, C.; Zou, Q.; Zhu, C.; Yan, F. Influence of coupled effect among flaw parameters on strength characteristic of precracked specimen: Application of response surface methodology and fractal method. *J. Nat. Gas Sci. Eng.* **2015**, *26*, 857–866. [\[CrossRef\]](#)
12. Sagong, M.; Bobet, A. Coalescence of multiple flaws in a rock-model material in uniaxial compression. *Int. J. Rock Mech. Min.* **2002**, *39*, 229–241. [\[CrossRef\]](#)
13. Zhao, Y.; Gao, Y.; Wu, S.; Chen, L.; Zhang, C. Experimental and numerical study of failure characteristics of brittle rocks with single internal 3D open-type flaw. *Acta Geotech.* **2021**, *16*, 3087–3113. [\[CrossRef\]](#)
14. Yang, S.-Q.; Jing, H.-W. Strength failure and crack coalescence behavior of brittle sandstone samples containing a single fissure under uniaxial compression. *Int. J. Fract.* **2011**, *168*, 227–250. [\[CrossRef\]](#)
15. Li, H.; Wong, L.N.Y. Influence of flaw inclination angle and loading condition on crack initiation and propagation. *Int. J. Solids Struct.* **2012**, *49*, 2482–2499. [\[CrossRef\]](#)
16. Wong, R.H.; Chau, K. Crack coalescence in a rock-like material containing two cracks. *Int. J. Rock Mech. Min. Sci.* **1998**, *35*, 147–164. [\[CrossRef\]](#)
17. Yang, S.Q.; Yang, D.S.; Jing, H.W.; Li, Y.H.; Wang, S.Y. An experimental study of the fracture coalescence behaviour of brittle sandstone specimens containing three fissures. *Rock Mech. Rock Eng.* **2012**, *45*, 563–582. [\[CrossRef\]](#)
18. Zhang, X.-P.; Liu, Q.; Wu, S.; Tang, X. Crack coalescence between two non-parallel flaws in rock-like material under uniaxial compression. *Eng. Geol.* **2015**, *199*, 74–90. [\[CrossRef\]](#)
19. Xu, G.; Hu, X.; Tang, R.; Hou, Z. Fracture evolution of transversely isotropic rocks with a pre-existing flaw under compression tests based on moment tensor analysis. *Acta Geotech.* **2021**, *17*, 169–203. [\[CrossRef\]](#)
20. Wong, L.; Einstein, H. Systematic evaluation of cracking behavior in specimens containing single flaws under uniaxial compression. *Int. J. Rock Mech. Min. Sci.* **2009**, *46*, 239–249. [\[CrossRef\]](#)
21. Wong, L.N.Y.; Einstein, H.H. Crack coalescence in molded gypsum and carrara marble: Part 1. macroscopic observations and interpretation. *Rock Mech. Rock Eng.* **2009**, *42*, 475–511. [\[CrossRef\]](#)
22. Zhang, K.; Cao, P.; Ma, G.; Wang, W.; Fan, W.; Li, K. Strength, fragmentation and fractal properties of mixed flaws. *Acta Geotech.* **2016**, *11*, 901–912. [\[CrossRef\]](#)
23. Liu, G.; Sun, W.; Lowinger, S.M.; Zhang, Z.; Huang, M.; Peng, J. Coupled flow network and discrete element modeling of injection-induced crack propagation and coalescence in brittle rock. *Acta Geotech.* **2019**, *14*, 843–868. [\[CrossRef\]](#)
24. Sun, W.B.; Du, H.Q.; Zhou, F.; Shao, J.L. Experimental study of crack propagation of rock-like specimens containing conjugate fractures. *Geomech. Eng.* **2019**, *17*, 323–331. [\[CrossRef\]](#)
25. Maji, A.K.; Shah, S.P. Application of acoustic emission and laser holography to study microfracture in concrete. *ACI Symp. Publ.* **1989**, *112*, 83–110.
26. Janeiro, R.P.; Einstein, H.H. Experimental study of the cracking behavior of specimens containing inclusions (under uniaxial compression). *Int. J. Fract.* **2010**, *164*, 83–102. [\[CrossRef\]](#)
27. Liu, B.; Sun, Y.; Wang, B.; Han, Y.; Zhang, R.; Wang, J. Effect of water content on mechanical and electrical characteristics of the water-rich sandstone during freezing. *Environ. Earth Sci.* **2020**, *79*, 236–249. [\[CrossRef\]](#)
28. Jia, H.; Zi, F.; Yang, G.; Li, G.; Shen, Y.; Sun, Q.; Yang, P. Influence of pore water (ice) content on the strength and deformability of frozen argillaceous siltstone. *Rock Mech. Rock Eng.* **2020**, *53*, 967–974. [\[CrossRef\]](#)
29. Jia, H.; Ding, S.; Wang, Y.; Zi, F.; Sun, Q.; Yang, G. An NMR-based investigation of pore water freezing process in sandstone. *Cold Reg. Sci. Technol.* **2019**, *168*, 102893. [\[CrossRef\]](#)
30. Sun, Q.; Dong, Z.; Jia, H. Decay of sandstone subjected to a combined action of repeated freezing–thawing and salt crystallization. *Bull. Eng. Geol. Environ.* **2019**, *78*, 5951–5964. [\[CrossRef\]](#)
31. Jia, H.; Xiang, W.; Krautblatter, M. Quantifying rock fatigue and decreasing compressive and tensile strength after repeated freeze-thaw cycles. *Permafr. Periglac. Process.* **2015**, *26*, 368–377. [\[CrossRef\]](#)
32. Jia, H.; Leith, K.; Krautblatter, M. Path-dependent frost-wedging experiments in fractured, low-permeability granite. *Permafr. Periglac. Process.* **2017**, *28*, 698–709. [\[CrossRef\]](#)
33. Ruedrich, J.; Kirchner, D.; Siegesmund, S. Physical weathering of building stones induced by freeze–thaw action: A laboratory long-term study. *Environ. Earth Sci.* **2011**, *63*, 1573–1586. [\[CrossRef\]](#)
34. Yang, L.; Jia, H.; Han, L.; Zhang, H.; Tang, L. Hysteresis in the ultrasonic parameters of saturated sandstone during freezing and thawing and correlations with unfrozen water content. *J. Rock Mech. Geotech.* **2021**, *13*, 1078–1092. [\[CrossRef\]](#)
35. Jia, H.; Han, L.; Zhao, T.; Sun, Q.; Tan, X. Strength and the cracking behavior of frozen sandstone containing ice-filled flaws under uniaxial compression. *Permafr. Periglac. Process.* **2022**, *33*, 160–175. [\[CrossRef\]](#)
36. Wang, T.; Sun, Q.; Jia, H.; Ren, J.; Luo, T. Linking the mechanical properties of frozen sandstone to phase composition of pore water measured by LF-NMR at subzero temperatures. *Bull. Eng. Geol. Environ.* **2021**, *80*, 4501–4513. [\[CrossRef\]](#)

**Disclaimer/Publisher’s Note:** The statements, opinions and data contained in all publications are solely those of the individual author(s) and contributor(s) and not of MDPI and/or the editor(s). MDPI and/or the editor(s) disclaim responsibility for any injury to people or property resulting from any ideas, methods, instructions or products referred to in the content.